Journal of Biomedical Optics

BiomedicalOptics.SPIEDigitalLibrary.org

Characterization of healthy and nonmelanoma-induced mouse utilizing the Stokes–Mueller decomposition

Dan Linh Le
Trinh Ngoc Huynh
Dat Tan Nguyen
Toi Van Vo
Thi-Thu-Hien Pham

SPIE.

Dan Linh Le, Trinh Ngoc Huynh, Dat Tan Nguyen, Toi Van Vo, Thi-Thu-Hien Pham, "Characterization of healthy and nonmelanoma-induced mouse utilizing the Stokes–Mueller decomposition," *J. Biomed. Opt.* **23**(12), 125003 (2018), doi: 10.1117/1.JBO.23.12.125003.

Characterization of healthy and nonmelanoma-induced mouse utilizing the Stokes–Mueller decomposition

Dan Linh Le,[a] Trinh Ngoc Huynh,[b] Dat Tan Nguyen,[a] Toi Van Vo,[a] and Thi-Thu-Hien Pham[a,*]
[a]International University—Vietnam National University HCMC, Department of Biomedical Engineering, Ho Chi Minh City, Vietnam
[b]University of Medicine and Pharmacy, Department of Pharmacognosy, Ho Chi Minh City, Vietnam

Abstract. Skin cancer is one of the most common cancers, including melanoma and nonmelanoma cancer. Melanoma can be easily detected by the observation of abnormal moles, but nonmelanoma signs and symptoms are not apparent in the early stages. We use the Stokes–Mueller matrix decomposition method to detect nonmelanoma at the early stage by decomposing the characteristics of polarized light interacting with normal and cancerous tissues. With this decomposition method, we extract nine optical parameters from biological tissues, namely the LB orientation angle (α), the LB phase retardance (β), the CB optical rotation angle (γ), the LD orientation angle (θ_d), the linear dichroism (D), the circular dichroism (R), the degrees of linear depolarization (e_1 and e_2), the degree of circular depolarization (e_3), and the depolarization index (Δ). The healthy skin and the induced nonmelanoma skin cancer of mice are analyzed and compared based on their optical parameters. We find distinctive ranges of values for normal skin tissue and nonmelanoma skin cancer, in which β and D in cancerous tissue are larger and nonmelanoma skin becomes less depolarized. This research creates an innovative solid foundation for the diagnosis of skin cancer in the future. [DOI: 10.1117/1.JBO.23.12.125003]

Keywords: skin cancer; mouse tumor; polarized light; Mueller matrix; Stokes polarimetry; tissue characterization.

Paper 180534R received Sep. 13, 2018; accepted for publication Nov. 27, 2018; published online Dec. 15, 2018.

1 Introduction

Our skin, the largest organ of our body, is the first line of defense for preventing microorganisms, chemicals, and UV light from directly damaging vulnerable inner organs. Overexposure to those pathogens, toxins, or rays, does harm to our skin, for example, sunburn, burns, and acne. Skin cancer is the worst scenario for not only your skin but also your body due to uncontrollable growth of tumor and metastasis; however, it is rising significantly globally, caused by increased outdoor activities and longevity, changing in clothing styles, ozone depletion, and immunosuppression in some cases.[1] Skin cancer includes melanoma and nonmelanoma skin cancer. Whereas melanoma skin cancer can be determined when suspicious moles appear, nonmelanoma signs and symptoms are unnoticeable in the early stages and take time to progress and be more evident, which delays proper treatment for the patient and lower survival rate. Accordingly, the early detection of nonmelanoma skin cancer is a must. On the other hand, for clinical evaluation of nonmelanoma, a biopsy is the gold standard. However, a biopsy is invasive, costly, and can result in the scar on the face or the neck.[2] The diagnosis of nonmelanoma skin cancer has been of great interest to the search for new noninvasive techniques. Currently, the optical diagnostic techniques were researched and applied by different approaches,[3] such as confocal microscopy,[4,5] optical coherence tomography,[6,7] and spectroscopy.[8]

Methods for specifying the true of skin pathologies noninvasively remain an unresolved question for the dermatology community. By utilizing the Mueller matrix decomposition method and Stokes polarimetry, we can extract the effective linear birefringence (LB), linear dichroism (LD), circular birefringence (CB), circular dichroism (CD), linear depolarization (L-Dep), and circular depolarization (C-Dep) properties of tissues or organs. The estimation of the LB of tissue provides an approach for noninvasive diagnosis of different obsessive diseases and thorough insight into the characteristics of the photoelasticity of human tissue.[9–11] Moreover, CB measurements of human blood indicate diabetes reliably.[12] CD analysis can classify different proteins,[13,14] whereas LD measurements of human tissue can diagnose tumor.[15] Additionally, valuable experience of the characteristics of tumor surface measurements can be obtained through analyzing linear depolarization parameters.[16]

Many studies have demonstrated that the Mueller matrix decomposition technique has potential for detailed inspection and analysis of biological samples. Lu and Chipman[17] proposed Mueller matrix decomposition methods for determining its diattenuation, retardance, and depolarization. Ghosh et al.[18] investigated the efficacy of a Mueller matrix decomposition methodology to extract the individual intrinsic polarimetry characteristics from a multiply scattering medium exhibiting simultaneous LB and optical activity. Wood et al.[19] applied a Monte Carlo model for polarized light propagation in birefringent, optically active, multiply scattering media for accurately representing the propagation of polarized light in biological tissue. Du et al.[20] examined the microstructure and optical properties of biological tissue samples by analyzing the backscattering Mueller matrix patterns. Martin et al.[21] compared normal and irradiated pig skin samples using the Mueller matrix decomposition methods developed by Lu and Chipman.[17] However, these above techniques are order dependent, so its

*Address all correspondence to Thi-Thu-Hien Pham, E-mail: ptthien@hcmiu.edu.vn

applications are limited. Azzam[22] proposed the differential matrix formalism for an anisotropic medium in parallelism with Jones' matrix formalism. Ossikovski[23,24] extended the differential matrix formalism for depolarization anisotropic media. Ortega-Quijano and Arce-Diego[25,26] proposed the differential Mueller matrix decomposition in the backward direction and was successfully applied to Mueller matrices measured in reflection and backscattering. Liao and Lo[27] proposed a hybrid model comprising differential and decomposition based Mueller matrices for extracting anisotropic parameters of turbid media regardless of the sequence. However, these differential Mueller matrix decomposition techniques described above were not able to extract all anisotropic parameters due to the complicated mathematical model. Pham and Lo[28–30] proposed a decoupled analytical technique based on forward Mueller matrix decomposition for extracting all effective LB, LD, CD, CB, L-Dep, and C-Dep parameters in a decoupled manner of turbid media by an advanced proposed analytical method. In this study, this proposed method to visualize skin pathologies using polarized light imaging is discussed. Based on the achievement in previous studies,[28–30] the validity of the technique is established by collecting the effective optical properties between the healthy tissues from 30 samples of 5 mice and skin cancer tissues from 72 samples of 12 mice. This technology will assist doctors as well as dermatologists in making a quick assessment of skin pathologies.

2 Methodology

2.1 *Stokes–Mueller Matrix Decomposition Method for Extracting Optical Parameters*

Based on previous studies, we applied the analytical technique of Pham and Lo[28–30] to extract nine effective parameters, including the LB orientation angle (α), the LB phase retardance (β), the CB optical rotation angle (γ), the LD orientation angle (θ_d), the linear dichroism (D), the circular dichroism (R), the degrees of linear depolarization (e_1 and e_2), the degree of circular depolarization (e_3), and the depolarization index (Δ), of healthy and skin cancer samples.

For a biomedical sample, the output Stokes vector, S_c, has the form

$$S_c = \begin{bmatrix} S_0 \\ S_1 \\ S_2 \\ S_3 \end{bmatrix}_c = M_\Delta M_{lb} M_{cb} M_{ld} M_{cd} \hat{S}_c = \begin{pmatrix} m_{11} & m_{12} & m_{13} & m_{14} \\ m_{21} & m_{22} & m_{23} & m_{24} \\ m_{31} & m_{32} & m_{33} & m_{34} \\ m_{41} & m_{42} & m_{43} & m_{44} \end{pmatrix} \begin{pmatrix} \hat{S}_0 \\ \hat{S}_1 \\ \hat{S}_2 \\ \hat{S}_3 \end{pmatrix}_c, \quad (1)$$

where M_Δ, M_{lb}, M_{cb}, M_{ld}, and M_{cd} are the Mueller matrices for the depolarization, lb, cb, ld, and cd properties of the sample, respectively, and $\hat{S}_c$ is the input Stokes vector. In the methodology adopted in this study, the sample is radiated by four input linear polarization states (i.e., $\hat{S}_{0\ \mathrm{deg}} = [1, \ 0, \ 1, \ 0]^T$, $\hat{S}_{45\ \mathrm{deg}} = [1, \ 0, \ 1, \ 0]^T$, $\hat{S}_{90\ \mathrm{deg}} = [1, \ -1, \ 0, \ 0]^T$, and $\hat{S}_{135\ \mathrm{deg}} = [1, \ 0, \ -1, \ 0]^T$) and two input circular polarization lights (i.e., right-handed $\hat{S}_{\mathrm{RHC}} = [1, \ 0, \ 0, \ 1]^T$ and left-handed $\hat{S}_{\mathrm{LHC}} = [1, \ 0, \ 0, \ -1]^T$).

Noticeably, full details of the experimental procedure used to extract the various parameters are mentioned in Refs. 28–30. To sum up, the LB orientation angle (α), phase retardance (β), optical rotation angle (γ), LD orientation angle (θ_d), linear dichroism (D), circular dichroism (R), linear depolarization (e_1, e_2), and circular depolarization (e_3) can be extracted using Stokes–Mueller technique from Refs. 28–30. Notably, this methodology does not require the alignment of the principal birefringence axes and diattenuation axes. Although only four different input polarization lights, namely three linear polarization lights (i.e., $\hat{S}_{0\ \mathrm{deg}}$, $\hat{S}_{45\ \mathrm{deg}}$, and $\hat{S}_{90\ \mathrm{deg}}$) and one circular polarization lights (i.e., $\hat{S}_{\mathrm{RHC}}$), are enough for obtaining all elements of Mueller matrix, the extra two input polarization states (i.e., $\hat{S}_{135\ \mathrm{deg}}$ and $\hat{S}_{\mathrm{LHC}}$) further improve the experimental results. Moreover, the ability of the analytical model for extracting all the optical parameters of interest over the measurement ranges was verified using an analytical simulation and error analysis technique. Thus, the analytical model yielded accurate results even when the output Stokes parameters had errors in the range of ± 0.005, or the samples had the minimum measurement of birefringence or dichroism.[28–30]

2.2 *Experimental Setup*

The polarized light system included a helium–neon laser (wavelength of 632.8 nm, power <5 mW), a quarter-wave plate, polarizers, and a Stokes polarimeter to characterize the LB, LD, CB, CD, L-Dep, and C-Dep properties of turbid media. In performing the experiments, the input light was provided by a frequency-stable He–Ne laser (HNLS008R, Thorlabs Co.) with a central wavelength of 633 nm. Also, a polarizer (GTH5M, Thorlabs Co.) and a quarter-wave plate (QWP0-63304-4-R10, CVI Co.) were used to produce four linear polarization lights (0 deg, 45 deg, 90 deg, and 135 deg) and two circular polarization lights (right-handed and left-handed). Finally, a neutral density filter (NDC-100-2, ONSET Co.) was used to ensure that each of the input polarization lights had the equal intensities. The output Stokes parameters were computed from the intensity measurements obtained using a commercial Stokes polarimeter (PAX5710, Thorlabs Co.) at a sampling rate of 33.33 samples per second. A minimum of 1024 data points was obtained for each sample. Of these data points, 100 points were chosen and used to calculate the mean value of each effective parameter. Figure 1 shows the installation of the system. The samples were placed between the polarizer and detector by being fixed to a side stand. It is noted that the error analysis

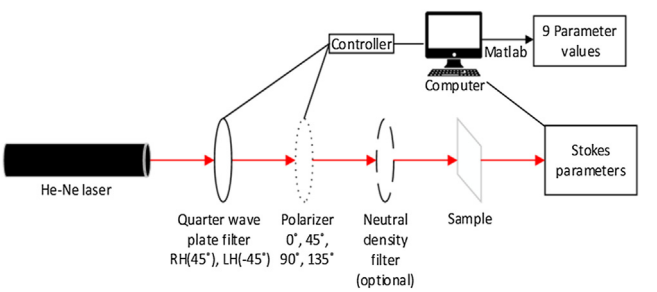

Fig. 1 Schematic illustration of a model of measurement.

of the proposed system was performed and described in detail in Ref. 29. The analytical model yields accurate results even when the output Stokes parameters have errors in the range −0.005 to +0.005 or the samples have very low values of birefringence or dichroism.[29] Furthermore, the reliability of the proposed system was evaluated using different optical samples, namely a quarter-wave plate (QWP0-633-04-4-R10, CVI Co.); a half-wave plate (QWP0-633-04-2-R10, CVI Co.), a polarizer (GTH5M, Thorlabs Co.); a baked polarizer (LLC2-82-18S, OPTIMAX Co.); a polarization controller; a composite sample comprising a quarter-wave plate, a half-wave plate, and a polarizer; and a depolarizer (DEQ-1N in ONSET Co.).[28,29]

3 Sample Preparation

3.1 *Materials*

7,12-dimethylbenz[a]anthracene (DMBA) (≥95%) and croton oil were purchased from Sigma–Aldrich Co. (Germany), meanwhile Hematoxylin and Eosin stain were bought from

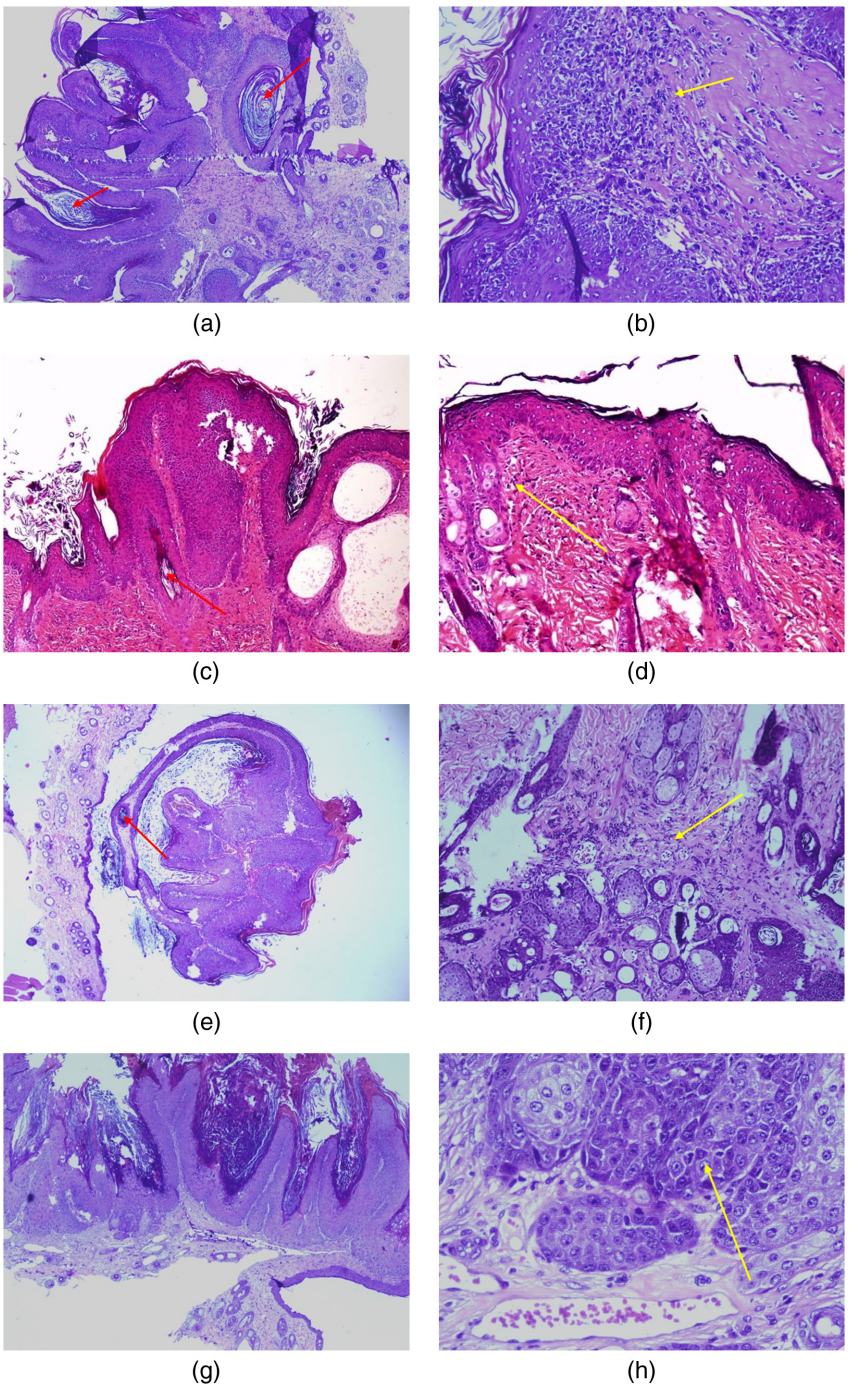

Fig. 2 Histopathological results of nonmelanoma-induced mice. (a) and (b) Sample 1, (c) and (d) sample 15, e and (f) sample 9, and (g) and (h) sample 10.

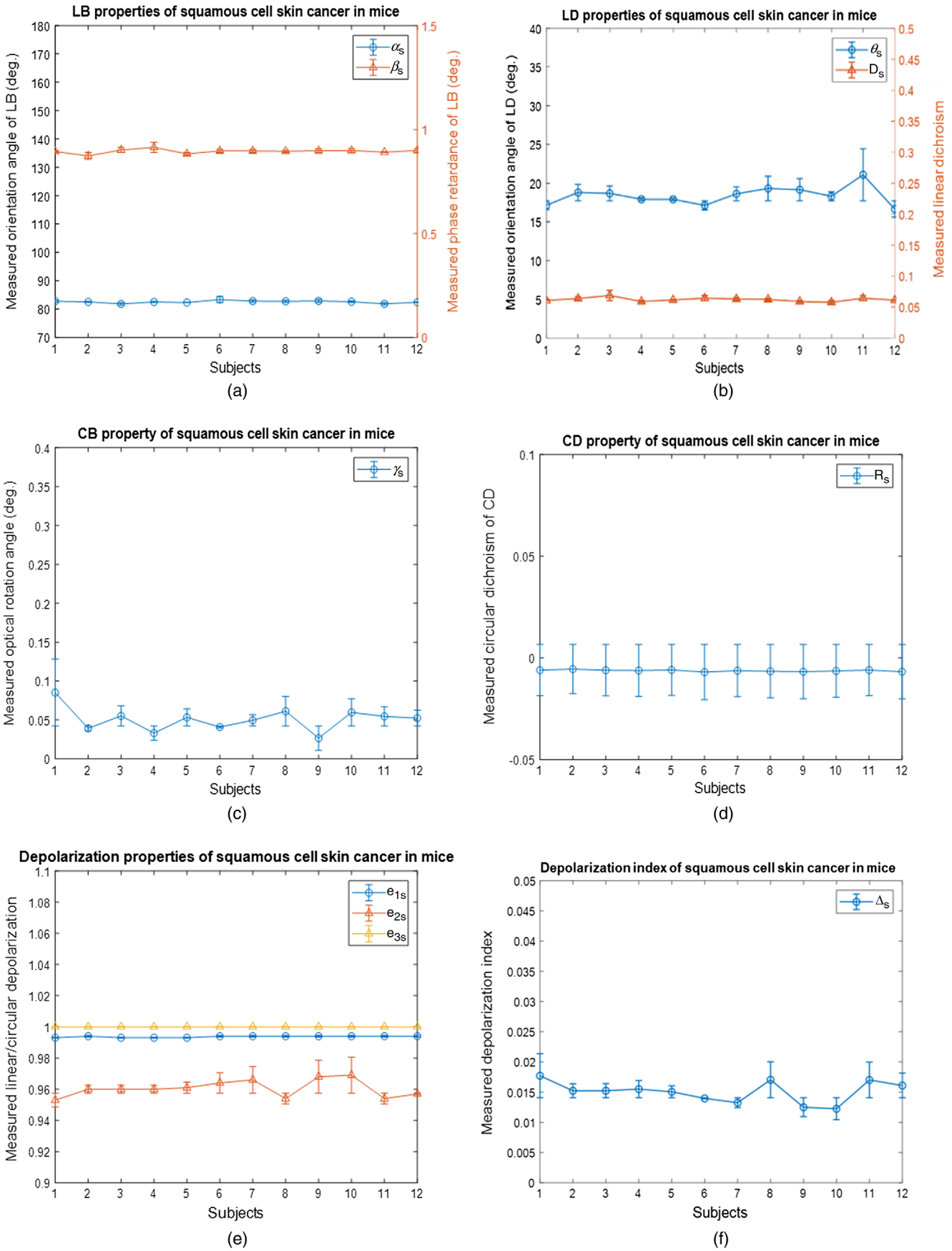

Fig. 3 Effective properties of (a) orientation angles of LB (α_S) and phase retardations of LB (β_S); (b) orientation angle of LD (θ_S) and linear dichroism (D_S); (c) optical rotation of CB (γ_S); (d) circular dichroism (R_S); (e) depolarization (e_{1S}, e_{2S}, and e_{3S}); and (f) depolarization index of squamous cell skin cancer in mice.

Sigma–Aldrich Co.. Ethanol, xylene, and acetic acid ($CH3COOH \geq 99.5\%$) were purchased from Xilong, China.

3.2 *Experimental Animals*

We performed the experiment on 17 healthy male Swiss albino mice (25 to 30 g) purchased from Institute of Vaccine and Medical Biology of Nha Trang city, IVAC (Vietnam). Mice were individually housed per cage and were acclimatized to a 12-h light–dark cycle for at least one week before each experiment. The animals had free access to food pellets (IVAC, Vietnam) and water ad libitum. One day before the treatment, the dorsal skin of mice was shaved for an ~ 2 cm $\times$ 2 cm area. All experimental protocols were conducted under the agreement of the scientific committee, specialty of Pharmacology and Clinical Pharmacy, Faculty of Pharmacy, University of Medicine and Pharmacy at the Ho Chi Minh City, Vietnam (Number 03-2016/QĐ-SĐHD).

3.3 *Two-Stage Chemical Carcinogenesis Protocol*

The cutaneous tumors were initiated on 12 mice by a single application on the dorsal shaved skin 50 μL of a 0.2% DMBA solution prepared in acetone (equivalent to 100 μg DMBA per mouse). Two weeks later, 50 μL of a 2% croton oil solution prepared in acetone (equivalent to 1 mg croton oil per mouse) was topically applied two times weekly until the end of the experiment. At the 20th week, mice were euthanized by CO_2 asphyxiation, and skin samples were then isolated and fixed in 10% formalin. Tissues were embedded in paraffin wax for further experiment.

3.4 *Optical Characterization*

The samples were sectioned with microtome with the thickness of 5 μm and embedded on Quartz slides. The slides were then analyzed using the polarized light system mentioned above.

3.5 *Histopathological Analysis*

Cancerous tissue samples were sectioned with microtome with the thickness of 5 μm and stained with Haematoxylin and Eosin (H&E) stain. Stained slides were observed under a light microscope for histopathological analysis.

4 Results

4.1 *Histopathological Validation of Pathology*

Figure 2 shows the histopathological results of nonmelanoma-induced mice. To be specific, there is the existence of abnormal squamous cells and the invasion of those cells from the epidermis to the dermis (yellow arrow). In Figs. 2(a), 2(c), and 2(e), keratin accumulates and appears as keratin pearls (red arrow). Furthermore, the thickness of the epidermis increases massively, and no borderline between epidermis and dermis has shown. These characteristics validate our induction of nonmelanoma skin cancer (squamous cell carcinoma) on mice.

4.2 *Optical Properties of Nonmelanoma Tumors*

The results of nine effective properties of nonmelanoma skin cancer in mice are shown in Fig. 3. Most of the optical characteristics extracted from 12 subjects show similarity, except orientation angle of LD (θ_S) and optical rotation of CB (γ_S). Specifically, in Fig. 3(a), orientation angles of LB (α_S) are all close to 82 deg, whereas phase retardations of LB (β_S) are around 0.9 deg. Also, in Figs. 3(b) and 3(d), measured linear dichroisms (D_S) are nearly 0.06, whereas measured circular dichroisms (R_S) are almost -0.006. Figure 3(e) shows that all of the linear depolarization (e_{1S} and e_{2S}) and circular depolarization are close to 0.99, 0.96, and 1, respectively. However, depolarization indices calculated from (e_{1S}, e_{2S}, and e_{3S}) show slight variation ranging from 0.20 to 0.28. Noticeably, in Figs. 3(b) and 3(c), most of the subjects showed properties of the orientation angle of LD (θ_S) at almost 20 deg, and the optical rotation angle of CB (γ_S) varied among the mice ranging from 0.025 deg to 0.08 deg.

Table 1 shows the values of optical properties for the control samples and nonmelanoma skin cancer. The values were the average, and the standard deviation from 6 measurement points on each of 72 samples extracted from 12 cancer subjects and each of 30 samples extracted from 5 normal subjects are calculated as shown in Table 1.

The detailed results of major effective properties including phase retardance and orientation angle of LB, optical rotation angle of CB, LD, and depolarization index comparing healthy tissue and squamous cell skin cancer in mice are shown in Figs. 4–6. Birefringence, LD, and depolarization index are the representatives of three fundamental polarization properties of the medium: retardance, diattenuation, and depolarization, respectively.

Figure 4 shows that the values of measured orientation angle and phase retardance of LB in mice with squamous cell skin cancer are significantly lower than in normal mice, where the figures of α and β among normal mice are around 145 deg and 1.26 deg; the ones in cancer mice are ~ 82.6 deg and 0.9 deg, respectively. As shown in Fig. 5, the tendency of CB is similar with that of LB. The optical rotation angles of CB, γ, of normal samples fluctuate around 0.88 deg while

Table 1 Optical properties of normal and squamous cell skin cancer in mice.

		α	β	γ	θ_d	D	R	e_1	e_2	e_3	Δ
Squamous cell mouse skin cancer	Mean	82.56	0.90	0.05	18.69	0.06	−0.006	0.99	0.96	1	0.015
	SD[a]	0.43	0.03	0.02	0.63	0.003	0.0004	0.003	0.005	0	0.02
Control mouse	Mean	145.7	1.26	0.88	60.24	0.13	−0.014	0.99	−0.98	1	0.011
	SD[a]	29.0	0.04	0.53	5.87	0.006	0.13	0.009	0.01	0	0.03

[a]SD: Standard deviation

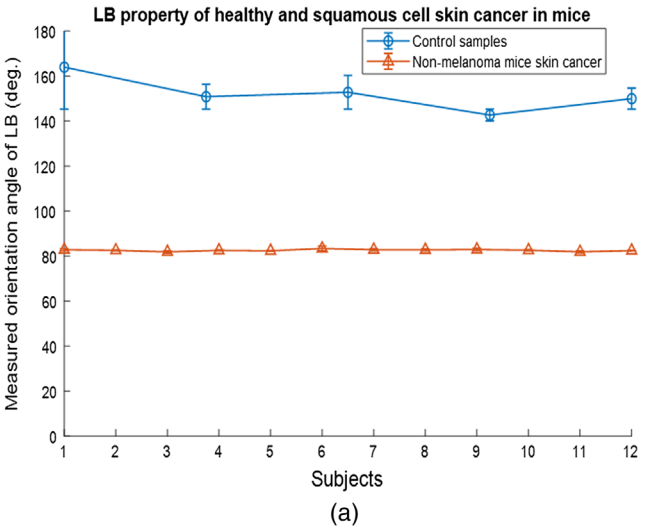

Fig. 4 LB properties of healthy and squamous cell skin cancer in mice (a) orientation angles of LB (α_S) and (b) phase retardations of LB (β_S).

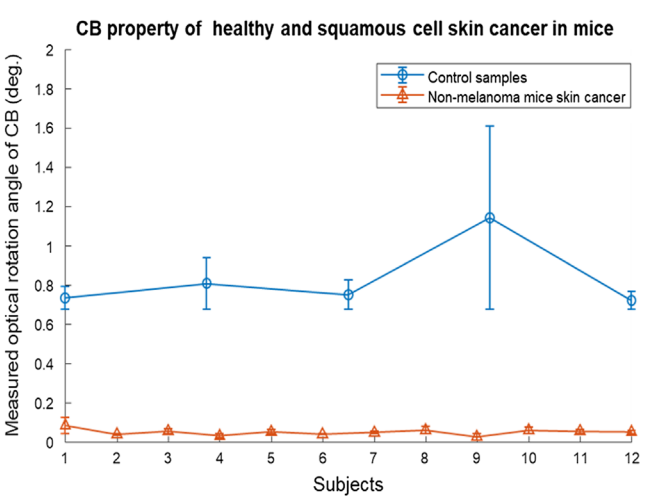

Fig. 5 CB properties of healthy and squamous cell skin cancer in mice.

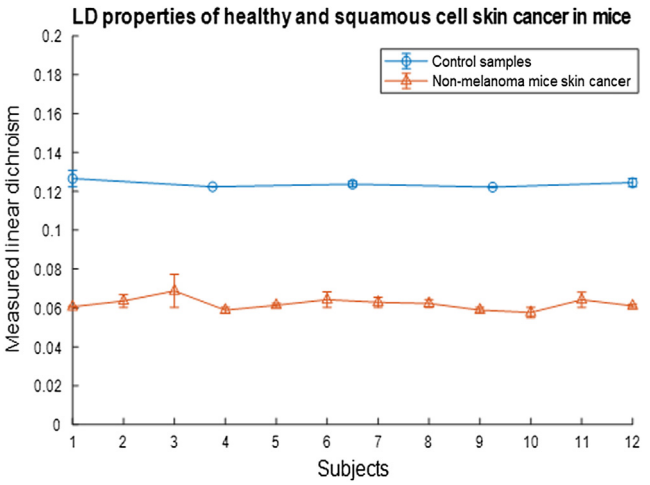

Fig. 6 LD of squamous cell skin cancer in mice.

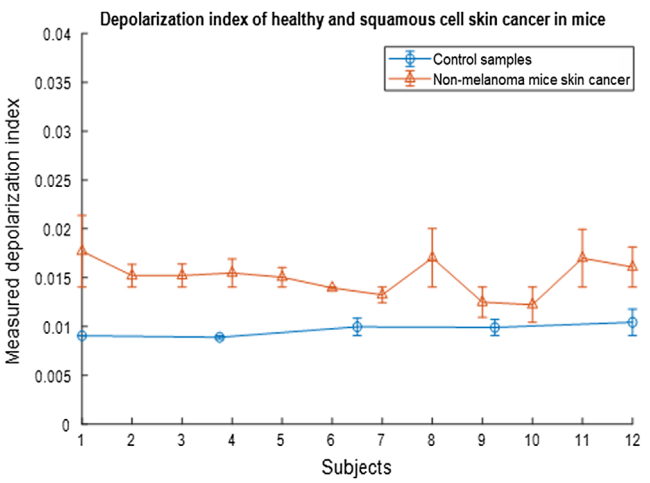

Fig. 7 Depolarization index of healthy and squamous cell skin cancer in mice.

that of cancerous samples is close to 0.05 deg. Remarkably, there is a normal skin sample with high γ and large standard deviation. The results of LD are in the same tendency with birefringence as shown in Fig. 6. The D of control samples is slightly below 0.13 deg, whereas those of cancer mice fluctuate around 0.06 deg. The trend for the depolarization index of healthy and cancer mice is opposite as shown in Fig. 7. The values in 12 samples of cancer mice fluctuate around 0.015, whereas normal skin tissues have more depolarization (around 0.011). Wide error bars that appear in several subjects indicate the measured values are relatively dispersed. In general, the five parameters analyzed have provided a significant distinction between squamous cell skin cancer and healthy skin in mice.

5 Discussion

In this study, we utilize the Stokes–Mueller matrix decomposition method to interpret the Mueller matrix into effective LB, LD, CD, CB, L-Dep, and C-Dep parameters of nonmelanoma-induced skin and normal skin in mice. The properties extracted are used to differentiate nonmelanoma cancer from the healthy skin in an effort to validate our effective approach for early detection of disease.

Retardance refers to birefringence, which are the properties of anisotropic materials. In the tissue, anisotropy mainly originates from structures, such as collagen fibrils and elastin fibers. Therefore, the morphology and structure of collagen and elastin in the extracellular matrix determine the magnitude of retardance and birefringence properties. When cancerous tumors develop in the body, numerous changes in collagen components occur, for example, deposition of collagen fibrils resulting from an increased number of fibroblasts, the production of proteolytic enzymes for cancer invasion.[31] This supports our findings that the growth of nonmelanoma skin cancer in mice lowers the values of LB and CB considerably as shown in Fig. 4. It means that the anisotropy of collagen decreases, caused by the alteration of the collagen fibril structure. On the other hand, diattenuation, the phenomenon that the transmittance of tissue depending on the state of polarization of incident light, characterized through measured dichroism is also dependent on anisotropy. In other words, anisotropy causing retardance also results in diattenuation.[32] Analogously, as the decreasing anisotropic properties of nonmelanoma skin cancer and the reasons for it are mentioned above, it is feasible that the results of measured dichroism of cancer samples are less than ones of normal samples. In addition to distinctive properties of nonmelanoma skin cancer in retardance and diattenuation, the reduction of depolarization is considerable. This can result from high cellular density, where cell nuclei are connected with the scattering of light.[33] Additionally, as the growth of abnormal cells of each subject and the cell density of each site may not be the same, it is understandable that there is a variation in depolarization and its standard deviation in cancer subjects. However, it can be observed that values of depolarization of cancerous tissue may overlap ones of normal tissue and the difference between average values seems to be minor, which may be because of our laser wavelength. Wang et al. found that the higher wavelength light results in the greater overlapping, but less variation of depolarization index, which suggests that the interaction of nonmelanoma with other wavelengths should be investigated.[16] Basically, this study indicates a comprehensive collection of effective parameters of normal and nonmelanoma murine skin, which can be used as a reference for further research in the future.

6 Conclusion

The research has revealed the polarization characteristics of nonmelanoma skin cancer in mice using the decoupled analytical technique based on Stokes polarimetry and Mueller matrix decomposition method. Thanks to the powerful technique, full sets of effective optical parameters consisting of LB, LD, CB, CD, L-Dep, and C-Dep were extracted for nonmelanoma differentiation. All obtained results came out as the expectation that, based on a consistent experiment, was done on our previous studies that have confirmed the reliability of the method. Although the method remains a number of limitations in sample preparation, sensitivity, and irrelevant optical alignment for clinical study, the experimental results show an excellent distinctiveness between nonmelanoma cancerous skin cancer and healthy skin in the aspects of retardance and diattenuation. Depolarization properties of nonmelanoma murine skin, on the other hand, are distinguishable but not significant. To sum up, our study provides basic evidence of a potential and noninvasive approach to detect nonmelanoma skin cancer at early stages.

Disclosures

The authors declare that they have no relevant financial interests in the paper and no other potential conflicts of interest.

Acknowledgments

The authors gratefully acknowledge the financial support provided to this study by Vietnam National Foundation for Science and Technology Development (NAFOSTED) under Grant No. 103.03-2016.86.

References

1. U. Leiter, T. Eigentler, and C. Garbe, "Epidemiology of skin cancer," *Adv. Exp. Med. Biol.* **810**, 120–140 (2014).
2. N. Eisemann et al., "Non-melanoma skin cancer incidence and impact of skin cancer screening on incidence," *J. Invest. Dermatol.* **134**, 43–50 (2014).
3. M. A. Calin et al., "Optical techniques for the noninvasive diagnosis of skin cancer," *J. Cancer Res. Clin. Oncol.* **139**, 1083–1104 (2013).
4. J. Malvehy and G. Pellacani, "Dermoscopy, confocal microscopy and other non-invasive tools for the diagnosis of non-melanoma skin cancers and other skin conditions," *Acta Derm. Venereol.* **97**(218), 22–30 (2017).
5. Y. Zhou et al., "Handheld photoacoustic microscopy to detect melanoma depth in vivo," *Opt. Lett.* **39**, 4731–4744 (2014).
6. Y.-Q. Xiong et al., "Optical coherence tomography for the diagnosis of malignant skin tumors: a meta-analysis," *J. Biomed. Opt.* **23**, 020902 (2018).
7. L. Themstrup et al., "Optical coherence tomography imaging of nonmelanoma skin cancer undergoing photodynamic therapy reveals subclinical residual lesions," *Photodiagn. Photodyn. Ther.* **11**, 7–12 (2014).
8. K. Kong et al., "Raman spectroscopy for medical diagnostics—from in-vitro biofluid assays to in-vivo cancer detection," *Adv. Drug Delivery Rev.* **89**, 121–134 (2015).
9. J. F. De Boer et al., "Two-dimensional birefringence imaging in biological tissue by polarization-sensitive optical coherence tomography," *Opt. Lett.* **22**, 934–936 (1997).
10. D. J. Maitland and J. T. Walsh, "Quantitative measurements of linear birefringence during heating of native collagen," *Lasers Surg. Med.* **20**, 310–318 (1997).
11. P. J. Wu and J. T. Walsh, "Stokes polarimetry imaging of rat tail tissue in a turbid medium: degree of linear polarization image maps using incident linearly polarized light," *J. Biomed. Opt.* **11**, 014031 (2006).
12. P. Sun et al., "Mueller matrix decomposition for determination of optical rotation of glucose molecules in turbid media," *J. Biomed. Opt.* **19**, 046015 (2014).
13. S. M. Kelly, T. J. Jess, and N. C. Price, "How to study proteins by circular dichroism," *Biochim. Biophys. Acta* **1751**, 119–139 (2005).
14. N. A. Swords and B. A. Wallace, "Circular-dichroism analyses of membrane proteins: examination of environmental effects on bacteriorhodopsin spectra," *Biochem J.* **289**(1), 215–219 (1993).
15. A. Angelskaya et al., "Manifestations of linear dichroism changes in cancer biotissues," *Rom. Rep. Phys.* **65**(3), 1052–1062 (2013).
16. W. Wang et al., "Roles of linear and circular polarization properties and effect of wavelength choice on differentiation between ex vivo normal and cancerous gastric samples," *J. Biomed. Opt.* **19**, 046020 (2014).
17. S.-Y. Lu and R. A. Chipman, "Interpretation of Mueller matrices based on polar decomposition," *J. Opt. Soc. Am. A* **13**(5), 1106–1106 (1996).
18. N. Ghosh, M. F. G. Wood, and I. A. Vitkin, "Mueller matrix decomposition for extraction of individual polarization parameters from complex turbid media exhibiting multiple scattering, optical activity, and linear birefringence," *J. Biomed. Opt.* **13**(4), 044036 (2008).
19. M. F. G. Wood, X. Guo, and I. A. Vitkin, "Polarized light propagation in multiply scattering media exhibiting both linear birefringence and optical activity: Monte Carlo model and experimental methodology," *J. Biomed. Opt.* **12**(1), 014029 (2007).
20. E. Du et al., "Characteristic features of Mueller matrix patterns for polarization scattering model of biological tissues," *J. Innovative Opt. Health Sci.* **7**(1), 1350028 (2014).

21. L. Martin, G. Le Brun, and B. Le Jeune, "Mueller matrix decomposition for biological tissue analysis," *Opt. Commun.* **293**, 4–9 (2013).
22. R. M. A. Azzam, "Propagation of partially polarized light through anisotropic media with or without depolarization: a differential 4×4 matrix calculus," *J. Opt. Soc. Am.* **68**(12), 1756–1767 (1978).
23. R. Ossikovski, "Differential matrix formalism for depolarizing anisotropic media," *Opt. Lett.* **36**(12), 2330–2330 (2011).
24. R. Ossikovski, "Differential and product Mueller matrix decompositions: a formal comparison," *Opt. Lett.* **37**(2), 220–222 (2012).
25. N. Ortega-Quijano and J. L. Arce-Diego, "Mueller matrix differential decomposition," *Opt. Lett.* **36**(10), 1942–1944 (2011).
26. N. Ortega-Quijano and J. L. Arce-Diego, "Mueller matrix differential decomposition for direction reversal: application to samples measured in reflection and backscattering," *Opt. Express* **19**(15), 14348–14353 (2011).
27. C. C. Liao and Y. L. Lo, "Extraction of anisotropic parameters of turbid media using hybrid model comprising differential and decomposition based Mueller matrices," *Opt. Express* **21**(14), 16831–16853 (2013).
28. T.-T.-H. Pham and Y.-L. Lo, "Extraction of effective parameters of turbid media utilizing the Mueller matrix approach: study of glucose sensing," *J. Biomed. Opt.* **17**(9), 097002 (2012).
29. T.-T.-H. Pham and Y.-L. Lo, "Extraction of effective parameters of anisotropic optical materials using a decoupled analytical method," *J. Biomed. Opt.* **17**(2), 025006 (2012).
30. T.-T.-H. Pham et al., "Optical parameters of human blood plasma, collagen, and calfskin based on the Stokes-Mueller technique," *Appl. Opt.* **57**, 4353–4359 (2018).
31. J. Qi and D. S. Elson, "Mueller polarimetric imaging for surgical and diagnostic applications: a review," *J. Biophotonics* **10**, 950–982 (2017).
32. S. B. Mehta, M. Shribak, and R. Oldenbourg, "Polarized light imaging of birefringence and diattenuation at high resolution and high sensitivity," *J. Opt.* **15**, 094007 (2013).
33. A. Pierangelo et al., "Ex-vivo characterization of human colon cancer by Mueller polarimetric imaging," *Opt. Express* **19**, 1582–1593 (2011).

Thi-Thu-Hien Pham received her BS degree in mechatronics from Ho Chi Minh City University of Technology-Vietnam National University, Ho Chi Minh City, Vietnam, in 2003 and her MS and PhD degrees in mechanical engineering from Southern Taiwan University of Technology and National Cheng Kung University, Tainan, Taiwan, in 2007 and 2012, respectively. Currently, she is a head of Biomedical Photonics Lab and a lecturer at Department of Biomedical Engineering, International University-Vietnam National University HCMC, Ho Chi Minh City, Vietnam. Her research interests are in the areas of polarized light-tissue studies, polarimetry, optical techniques in precision measurement to determine the optical properties of biosamples (glucose, collagen, and tumor) or cancer detection (skin, liver, and breast), noninvasive glucose measurement, cell/tissue characterization, laser/LED applications, and automatic control systems.

Biographies of the other authors are not available.